https://doi.org/10.5194/egusphere-2025-6442
Preprint. Discussion started: 20 February 2026

Title Page

Title: Four decades of full-depth profiles reveal layer-resolved drivers of reservoir thermal regimes and event-scale hypolimnetic warming

Chenxi Mi[1,2], Bo Gai[4], Xiangzhen Kong[1,3*], Yuzhe Jiang[3], Chun Ngai Chan[2], Karsten Rinke[3]

[1] State Key Laboratory of Lake and Watershed Science for Water Security, Nanjing Institute of Geography and Limnology, Chinese Academy of Sciences, Nanjing 211135, China

[2] Department of Biological Sciences, University of Lethbridge, Lethbridge, AB, T1K 3M4, Canada

[3] Department of Lake Research, UFZ - Helmholtz Centre for Environmental Research, Magdeburg 39114, Germany

[4] Swiss Federal Institute of Aquatic Science and Technology (Eawag), Surface Waters – Research and Management, Kastanienbaum, Switzerland

* Corresponding author:
Email: xzkong@niglas.ac.cn (X. Kong)

https://doi.org/10.5194/egusphere-2025-6442
Preprint. Discussion started: 20 February 2026

Abstract

Thermal structure shapes ecological dynamics in lakes and reservoirs. Yet full-profile temperature records over multi-decades remain scarce, constraining mechanistic understanding of depth-resolved thermal changes and subseasonal extremes (e.g., surface heat waves and late-season hypolimnetic warming). In this study, we focused on Rappbode Reservoir—Germany's largest drinking-water reservoir—and compiled four decades of high-resolution, full-depth temperature profiles with concurrent hydro-meteorological records that are rarely available for stratified systems. Building on these data, we developed a novel two-step analytical framework that integrates long-term monitoring and process-based modelling to yield a high-resolution, internally consistent dataset of spatiotemporal temperature dynamics. We then applied interpretable machine learning to quantify dominant external controls on depth-specific stratification dynamics and determine causal mechanisms governing late-stratification hypolimnetic warming. Our results suggested that influence of external drivers on the thermodynamic structure varied markedly with depth and stratification phase: stratification-strength metrics governed by atmospheric heat fluxes (i.e., surface temperature, vertical temperature difference, Schmidt stability) were controlled mainly by 30-day antecedent shortwave radiation and air temperature. For hypolimnetic temperatures and mixed-layer depth, outflow discharge turned out to be the primary driver during late stratification. Further analysis indicated that episodic hypolimnetic warming up to 10 °C in four specific years was mainly triggered by intensified deep withdrawals that weakened the density gradient and shortened the compensatory-flow pathway. The dual-perspective framework developed here—integrating

https://doi.org/10.5194/egusphere-2025-6442
Preprint. Discussion started: 20 February 2026

process-based and machine-learning approaches—is broadly transferable for analyzing ecological processes and supporting evidence-based management in stratified waters.

Keywords: Thermal stratification, Long-term temperature profiles, Hypolimnetic warming, CE-QUAL-W2, Interpretable machine learning methods

https://doi.org/10.5194/egusphere-2025-6442
Preprint. Discussion started: 20 February 2026

1. Introduction

Driven by solar heating, wind stress, and basin-scale hydrological exchanges, inland waters deeper than 7 m commonly develop seasonal thermal stratification—namely, a distinct vertical temperature gradient within the water column (Kirillin and Shatwell 2016). Solar warming of the surface layer, combined with limited turbulent mixing, generates a warm epilimnion while deep waters remain cold and form the hypolimnion. These two strata are separated by a region of sharp temperature gradients defined as metalimnion (Boehrer and Schultze 2009). This vertical structure controls oxygen and nutrient fluxes (Noori et al. 2023), governs redox-sensitive release of phosphorus from sediments (Deng et al. 2011), and shapes habitat availability for stenothermal organisms (Carr et al. 2019). It also modulates whole-lake emissions of carbon dioxide and methane, thereby shaping the lake's net role in the global carbon cycle (Mi et al. 2023a). Given the growing influence of climate warming and hydrological variability on stratification phenology (Mi et al. 2023b; Shatwell et al. 2019), a robust understanding of its long-term dynamics is indispensable for safeguarding water quality and designing adaptive management strategies.

Observations of high-resolution vertical lake water temperature dynamics over long periods are rarely available. Satellite sensors and nearshore infrared radiometers have provided continuous records of surface water temperature in lakes and reservoirs worldwide for over 40 years, enabling robust attribution of surface warming to air temperature, radiation, and wind forcing (Woolway et al. 2020). However, satellites measure only the surface skin (near-surface) temperature, and resolving vertical thermal structure still requires in-situ profilers. Globally, truly multi-decadal (>20 yr), depth-resolved temperature archives that meet basic

https://doi.org/10.5194/egusphere-2025-6442
Preprint. Discussion started: 20 February 2026

comparability criteria (harmonized vertical spacing, sub-monthly sampling frequency and consistent instrumentation over time) remain the exception rather than the rule, with available profile records frequently sparse and summer-biased, particularly below the metalimnion (Akbari et al. 2017). For example, under the Global Lake Temperature Collaboration (GLTC) initiative, Sharma et al. (2015) analyzed summer water temperatures from 291 lakes across different climate zones, and found that only ~20% of those lakes had temperature profile records for more than one year. Although a recent synthesis study compiled vertical temperature profiles from 153 lakes (Pilla et al. 2021) and quantitatively analyzed their thermal structure during stratified seasons, for most sites the record only consists of few profiles obtained during mid-summer, leaving large seasonal and inter-annual gaps. This global paucity of long-term, depth-resolved temperature records substantially limits the understanding of changes in internal thermal structure and their external forcings.

Mechanistic hydrodynamic lake models offer a principled means to generate such long-term time series of lake water temperatures at high spatial and temporal resolution (Dong et al. 2019). Following site-specific validation against routine monitoring data, such models enable physically consistent gap-filling to sub-daily resolution and longer-term extensions of vertical profiles, thereby supplying the vertically resolved context that short and sparse observations lack. However, robust mechanistic attribution of subsurface temperature variability and stratification intensity still hinges on multidecadal in situ observations, even when aided by model-based reconstructions (Anderson et al. 2021). Furthermore, deep-water thermal structure shows significantly lagged responses to decadal climate variability (e.g., the Pacific Decadal Oscillation and Atlantic Multidecadal Oscillation) and small-scale shear-induced

https://doi.org/10.5194/egusphere-2025-6442
Preprint. Discussion started: 20 February 2026

mixing (Kirillin and Shatwell 2016; Oleksy and Richardson 2021). If the monitoring record is shorter than a full decadal cycle, the corresponding analyses cannot reliably separate the influences of climate forcing and internal lake processes on the deep-water thermal structure (Boehrer and Schultze 2008). In turn, beyond complicating mechanistic diagnosis, the absence of sustained temperature profiles also undermines causal inference for vertically structured ecological responses, governed by the thermal regime (Meinson et al. 2016).

In addition, for deep temperate lakes/reservoirs, the thermocline acts as an effective thermal barrier, thus hypolimnetic temperatures remain low and stable—typically oscillating between 4 and 6 °C throughout the year, near the temperature of maximum-density of freshwater at 4°C (Boehrer and Schultze 2008). Recent studies, however, have documented late-stratification episodes in which the hypolimnion warms unexpectedly, with peak values occasionally exceeding 10 °C (Lewis Jr et al. 2019; Schwefel et al. 2025). Such deep-water thermal anomalies are being reported with increasing frequency, highlighting an emerging climate-driven phenomenon at depth (Woolway et al. 2025). Unlike the widely studied surface warming, these rare hypolimnetic warming events pose a disproportionate threat to ecosystem stability and drinking-water security. This is because hypolimnetic waters are characterized by low dissolved oxygen, strongly reducing conditions, and minimal water exchange, so that even slight warming can swiftly upset its delicate balance (Mi et al. 2023b). In fact, temperature increases in hypolimnion significantly accelerate biological and chemical reaction rates (roughly doubling per 10 °C, see Bouffard et al. (2013)), exponentially intensifying biogeochemical activity (Nkwalale et al. 2023). Consequently, a small warming of anoxic bottom waters can rapidly trigger cascading environmental responses–oxygen is consumed

https://doi.org/10.5194/egusphere-2025-6442
Preprint. Discussion started: 20 February 2026

faster and the sequestered nutrients, heavy metals, and greenhouse gases are abruptly mobilized (LaBrie et al. 2023). Given these risks, systematic analysis of deep-water warming is highly relevant to management. Yet, elucidating hypolimnetic thermal processes and identifying short-term anomalous events critically rely on sustained temperature measurements with sufficient vertical resolution (or highly resolved numerical simulations, see Boehrer and Schultze (2009)). As noted above, current observations of subsurface temperatures remain notably limited due to data availability and sampling frequency, hampering our understanding of the mechanisms underlying episodic hypolimnion warming events.

To fill these described research gaps, we used Rappbode Reservoir—the largest drinking-water reservoir in Germany—as a model system and compiled a unique 40-year, high-resolution archive of full-depth (0–70 m) temperature profiles. Leveraging the complementary strengths of process-based and data-driven approaches, we firstly established a site-validated CE-QUAL-W2 model which provides a physically consistent, gap-filled record of daily full-profile temperatures. We then applied an interpretable machine-learning layer—XGBoost coupled with SHAP—to obtain depth- and phase-resolved driver attributions of climate and operational forcings. Combined with the in situ monitoring, these components constitute a mechanistic–statistical framework that sharpens inference on interacting drivers, and isolates the dominant controls on deep-reservoir thermal dynamics. In this study, we seek to address the following key questions: (i) Which external forcings set full-column stratification strength, beyond surface warming?, (ii) How do the dominant drivers of water temperature dynamics vary with depth?, and (iii) Under what conditions is late-stratification hypolimnetic warming initiated and sustained? In addressing these questions, this study provides the first quantitative

https://doi.org/10.5194/egusphere-2025-6442
Preprint. Discussion started: 20 February 2026

explanation of the mechanisms triggering episodic hypolimnetic warming in stratified waters. Together, these advances yield a transferable mechanistic–statistical template in analyzing thermal evolution for inland waters, with conclusions that generalize well beyond this single system to stratified lakes and reservoirs.

2. Methods

2.1. Study site description

Located in the Harz Mountains, the Rappbode Reservoir (Fig. 1) is Germany's largest drinking-water reservoir and supplies raw water to more than one million people in the surrounding region (Rinke et al. 2013). The reservoir attains a maximum depth of 89 m (mean = 29 m), and the dam crest lies at 423.6 m a.s.l., with the total volume of 1.13×10^8 m³). Inflows are delivered by the Hassel and Rappbode pre-reservoirs and by a transfer tunnel from the Königshütte Reservoir (Mi et al. 2018). Six selective-withdrawal outlets are embedded in the dam at 345, 360, 370, 380, 390, and 400 m a.s.l.; the lowest outlet discharges to the downstream Wendefurth Reservoir, whereas the 360 m and 370 m intakes are routinely used for potable supply. With an annual residence time of roughly one year and the regional temperate climate, Rappbode exhibits a classic dimictic pattern—stable thermal stratification in summer and winter, and complete holomixis during spring and autumn. The national ban on phosphate-based detergents instituted three decades ago reduced total phosphorus from 0.16 mg L^{-1} in 1990 to the current level of approximately 0.02 mg L^{-1}, and the reservoir is now classified as meso- to oligotrophic status (Mi et al. 2022).

2.2. Long-term water temperature measurements

https://doi.org/10.5194/egusphere-2025-6442
Preprint. Discussion started: 20 February 2026

Since 1981, bi-weekly vertical temperature profiles have been taken at the deepest point immediately upstream of the Rappbode Dam (see Fig. 1), spanning the full water column from the surface to 70 m depth. Up to 2008, temperatures at discrete depths were measured with a thermometer inside an open cylinder sampler; from 2009 onward, measurements have been acquired with a Hydrolab DS5 multiparameter probe. Parallel deployments during the transition period confirmed statistical equivalence between the two methods (Wentzky et al. 2018). In this study, we used data from 1981 to 2019 (39 years in total), and after quality control, the record yields a depth–time matrix with year-round, across-season coverage and full water-column extent (0-70m), which serves as the basis for all subsequent analyses.

2.3. CE-QUAL-W2 model configuration

We developed an integrated framework linking four decades of water-temperature observations with process-based modeling and interpretable machine learning to elucidate the thermal evolution of the Rappbode Reservoir (Fig.1). Here, the process-based simulations were performed with CE-QUAL-W2 (hereafter W2, version 4.2.1), a laterally averaged, two-dimensional hydrodynamic model originally developed by the U.S. Army Corps of Engineers at 1975 (Cole and Wells 2006) and now maintained by the Department of Civil and Environmental Engineering at Portland State University. W2 is widely used as a standard tool for resolving hydrodynamic processes in lakes, reservoirs, and estuaries (e.g., Carr et al. 2019; Kobler et al. 2018), and is particularly well suited to systems dominated by longitudinal and vertical gradients such as the Rappbode Reservoir.

For Rappbode, the computational mesh comprises four branches subdivided into 106 longitudinal segments ($\Delta x = 100–400$m) and lateral sub-segments of 5–700m, yielding 3876

https://doi.org/10.5194/egusphere-2025-6442
Preprint. Discussion started: 20 February 2026

grid cells with a uniform 1m vertical resolution (Fig. S1). This discretization fully resolves the reservoir's bathymetry, enabling precise simulation of its morphological features. The model was driven by two sets of boundary conditions: (i) Hydrological forcing—daily inflow and outflow discharges together with inflow temperatures—was provided by the Rappbode Reservoir authority (Talsperrenbetrieb Sachsen-Anhalt); (ii) Meteorological forcing—hourly air temperature, relative humidity, wind speed and direction, incoming short-wave radiation, and cloud cover—was obtained from an monitoring buoy moored near the reservoir's centre (Rinke et al. 2013), with gaps infilled with records from the German Weather Service station at Harzgerode, ~15 km away from the reservoir. An intercomparison of Harzgerode and Rappbode Reservoir indicates a high degree of correlation in the meteorological records (see Mi et al. 2019 for more details). Simulations started on 1st January 1981 with an isothermal initial profile of 4 °C, representing a horizontally and vertically homogeneous state. A full description of the model configuration is presented in the Supplementary Information, as well as in our previous studies (see Mi et al. 2023b; Mi et al. 2020).

2.4. XGBoost description and modeling framework

XGBoost model description

Extreme Gradient Boosting (XGBoost) is an ensemble method that iteratively fits Classification-and-Regression Trees (CART) within a gradient-boosting framework. At each iteration *t*, the algorithm minimizes a regularized objective:

$$L^{t} = \sum_{i=1}^{n} l\left(y_i, \hat{y}_i^{t-1} + f_t(x_i)\right) + \sum_{k=1}^{t} \Omega(f_k) \quad (1)$$

$$\Omega(f) = \gamma T + \frac{1}{2}\lambda \sum_{j=1}^{T} w_j^2 \quad (2)$$

where $l(\cdot)$ is a twice-differentiable loss (squared error for regression), f_t is the *t*-th tree,

https://doi.org/10.5194/egusphere-2025-6442
Preprint. Discussion started: 20 February 2026

T is the number of leaves and w_j denotes leaf weights; γ and λ provide structural and weight regularization, respectively. Here, $\Omega(f)$ represents the regularization term that penalizes model complexity to prevent overfitting. By employing a second-order Taylor expansion of L^t, XGBoost obtains closed-form gain scores that guide an exact or histogram-based greedy search for the optimal split, while column subsampling and block-wise caching accelerate computation. This design yields three decisive benefits: (i) high accuracy, since second-order information markedly improves convergence; (ii) strong generalization, owing to L1/L2 shrinkage, learning-rate decay and stochastic sub-sampling; and (iii) computational efficiency, as multi-threaded and out-of-core execution scale to millions of observations and features on commodity hardware. Built-in cross-validation, early stopping and SHAP-based interpretability further underline XGBoost's suitability for handling small- to medium-sized and highly non-linear environmental data sets (Li et al. 2024; Lyu et al. 2019).

Description of model structure

We developed XGBoost models for predicting reservoir thermal structure according to daily outputs (1981–2019) from CE-QUAL-W2. Target variables comprise epilimnetic (5m depth), metalimnetic (15m depth), hypolimnetic (30m depth) and bottom (50m depth) temperatures, Schmidt Stability, the bottom-to-surface temperature difference and mixed-layer depth (see the Supplementary Materials for details on the last three indices and the post-processing methods). Since the above indices related to stratification dynamics are applicable only during thermal stratified period, therefore, the XGBoost model was constructed and analyzed exclusively for May–October. Guided by recent advances in

https://doi.org/10.5194/egusphere-2025-6442
Preprint. Discussion started: 20 February 2026

machine-learning modeling of lentic thermal structures (e.g., Bertone et al. 2015; Kreakie et al. 2021), the predictor set includes both the instantaneous and 30-day moving-average values of observed air temperature, relative humidity, wind speed and direction, incoming short-wave radiation, cloud cover and reservoir outflow discharge. Here, we included 30-day moving-average predictors to represent the cumulative component of atmospheric and hydraulic influences across depths, with the physical basis for this setting (epilimnetic thermal inertia τ) further detailed in Section 4.2. To be noted, our previous studies indicated that inflow discharge exerted only a marginal influence on the reservoir's thermal structure (Mi et al. 2020); thus, it was excluded as an input feature from the XGBoost model. All predictors included in the analysis were linearly de-trended, Z-score standardized and screened for collinearity ($|\rho| < 0.75$) to minimize feature redundancy (Deka and Weiner 2024).

The whole dataset was randomly split into training and testing subsets, with proportions of 80% and 20%, respectively. A 5-fold rolling-origin cross-validation combined with Bayesian optimization was employed to optimize the hyperparameters of the XGBoost model (e.g., eta, max_depth, subsample and colsample_bytree), and early stopping was invoked to minimize the root mean square error (RMSE) on the validation set. Model skill was then assessed on the full dataset with RMSE and the coefficient of determination (R^2), and SHapley Additive exPlanations (SHAP) values were calculated to quantify the relative contribution of each hydro-meteorological variable.

SHAP-based feature contribution analysis

In our XGBoost modeling framework, we quantified feature contributions using SHapley

https://doi.org/10.5194/egusphere-2025-6442
Preprint. Discussion started: 20 February 2026

Additive exPlanations (SHAP) values. SHAP is a model-agnostic interpretability framework rooted in cooperative game theory (Lundberg et al. 2020). It assigns each predictor a Shapley value calculated by evaluating the predictor's marginal contribution to model output across all possible subsets of input features (>0 pushes the prediction upward, <0 pulls it downward). We report the mean absolute SHAP for each feature as a measure of global importance. Here, SHAP distributions and effect sizes were visualized with beeswarm plots: the horizontal axis shows the SHAP value, and point color redundantly encodes the same measure on a single, shared scale (e.g., warm colors on the right indicate positive contributions, cool colors on the left indicate negative contributions, see Fig.9). Feature attributions computed via SHAP satisfy exact additivity, local accuracy, and consistency (null-feature property), providing a rigorous quantitative basis for disentangling the relative influence of hydrometeorological drivers on reservoir thermal dynamics. For more background on SHAP values, please refer to the Supplementary Material (Text S2).

3. Results

3.1. Model performance in simulating long-term reservoir hydrodynamics

The calibrated W2 accurately reproduced the interannual and seasonal water-level dynamics of Rappbode Reservoir over the 39-year period ($R^2 = 0.99$, see Fig.S2). The water level typically attains its annual maximum in spring (April–May, ~420 m a.s.l.) in response to increased rainfall, then declines sharply through summer driven by intensified evaporation and elevated drinking-water withdrawals. During winter, marked reductions in precipitation and inflows

https://doi.org/10.5194/egusphere-2025-6442
Preprint. Discussion started: 20 February 2026

caused the water-level to continually decline, reaching annual minima at the end of the season (e.g., 395 m a.s.l. in 2002). All of these characteristic fluctuations were satisfactorily captured by the model.

The model successfully captured spatiotemporal dynamics of the reservoir's thermal structure (such as thermocline depth and stratification onset (offset), see Fig.2). Simulated temperatures closely matched observations, with most points clustering along the 1:1 line ($R^2 = 0.95$; RMSE = 0.97 °C, see Fig. 2b). The simulated mean temperature (6.61°C) closely matched the observations (6.76°C) over the study period. More specifically, the simulation accuracy improved progressively with increasing depth, yielding RMSE of 1.27°C, 1.31°C, 0.75°C, and 0.59°C at depths of 5 m, 15 m, 30 m, and 50 m, respectively (Fig. 3). Both simulated and observed profiles demonstrate that intra-annual temperature amplitude diminishes sharply with depth, exceeding 15 °C at 5 m depth but falling below 10 °C (30m depth) and 8 °C (50m depth, see Fig. 3).

Additionally, simulated and observed temperatures exhibited highly consistent long-term trajectories (Fig. S3). At 5m depth, both series warmed significantly—0.05 K yr^{-1} for the observations and 0.06 K yr^{-1} for the simulations (Mann–Kendall test, $p < 0.05$)—with the mean epilimnetic temperature rising from ~15 °C in 1981–1985 to ~18 °C at the end of the record. By comparison, temperature at depths between 15m and 50m exhibited pronounced inter-annual variability but no statistically significant monotonic trend (Mann–Kendall test, $p > 0.05$, see Fig. S3).

3.2. Performance of XGBoost in simulating reservoir stratification dynamics

The calibrated XGBoost model successfully simulated the temperature dynamics in Rappbode

https://doi.org/10.5194/egusphere-2025-6442
Preprint. Discussion started: 20 February 2026

during the stratified period (Fig. 4). Trained on the daily CE-QUAL-W2 outputs as target values, the machine-learning model captured depth-specific temperature variations with high precision. Consistent with previous findings, the performance gradually improved with increasing depth—RMSE declined from 0.44 °C at 5 m to 0.16 °C at 50 m. The seasonal temperature pattern was also accurately represented by XGBoost: surface temperatures (5 m depth) followed a pronounced unimodal, bell-shaped curve that peaked in mid-July to early August, when the median daily temperature in both W2 and XGBoost simulations was ~19 °C, and cooled markedly at the onset (May) and offset (October) of the stratified period (Fig. 4). With increasing depth, the timing of peak temperature lagged progressively. At depths of 30 m and 50 m, temperatures rose continuously throughout the stratified period, reaching their maxima in October.

The stratification indices predicted by XGBoost are virtually congruent with the CE-QUAL-W2 outputs, as indicated by the tight clustering of points along the 1:1 line (Fig. 5). Specifically, Schmidt Stability was generally $< 1 \times 10^3$ J m^{-2} at the onset of stratification in May, increased steadily to a peak of $\sim 3 \times 10^3$ J m^{-2} in August, and declined thereafter, returning to the initial levels by October; this seasonal pattern closely paralleled that of the bottom-to-surface temperature difference (Fig. 5a). In contrast, the mixed-layer depth deepened throughout the stratified period: it remained < 10 m from May to August but reached approximately 20 m by October (Fig. 5b).

SHAP analysis of the XGBoost model indicates that epilimnetic temperature (5 m) is governed chiefly by the antecedent 30-day means of air temperature, dew-point temperature, and incident short-wave radiation (Fig. 6). With depth, the influence of air temperature

https://doi.org/10.5194/egusphere-2025-6442
Preprint. Discussion started: 20 February 2026

attenuates, ranking third, fourth, and fifth for the temperature at 15, 30, and 50 m depth, respectively, while short-wave radiation becomes the primary external driver below the surface layer. The importance of outflow discharge strengthens progressively down-profile, ranking eighth for epilimnetic temperature, fourth for temperature at 15 m depth, and second for temperature at 50 m depth. The relative importance of cloud cover as a driver of water temperature increased incrementally with depth, ranking sixth at depths of 5–30 m and fourth at 50 m. Wind speed and direction remain comparatively minor controls across all depths, ranking between sixth and eighth (Fig. 6). In sum, SHAP resolves a depth-structured forcing pattern: atmospheric control shifts from non-radiative terms in the epilimnion to short-wave radiation below the surface layer, while hydraulic withdrawal gains influence toward the hypolimnion.

Our results also indicated that both the bottom-to-surface temperature difference and Schmidt Stability are governed principally by the antecedent 30-day means of air temperature, incident short-wave radiation, and dew-point temperature (Fig. 7). By comparison, the mixed-layer depth was primarily driven by short-wave radiation over the preceding 30-day period, with outflow discharge and dew-point temperature ranking second and third, respectively. Cloud cover also significantly affected stratification dynamics, ranking fourth in importance for mixed-layer depth and fifth for Schmidt stability. In addition to antecedent forcings, instantaneous (same-day) conditions also exerted substantial control: specifically, same-day air temperature ranks fourth for its effect on both the bottom-to-surface temperature difference and Schmidt Stability (Fig. 7), whereas the same-day outflow discharge ranks fifth in modulating mixed-layer depth.

https://doi.org/10.5194/egusphere-2025-6442
Preprint. Discussion started: 20 February 2026

3.3. Mechanisms underlying the occurrence of elevated bottom-water temperatures in specific years

During the stratified season, hypolimnetic (50 m depth) temperatures in Rappbode Reservoir generally remains within the range of 4–6 °C. However, both in-situ profiles and W2 simulations reveal episodic warming to ~10 °C at the end of stratification (September–October) in 1981, 2001, 2002, and 2007 (Fig. 8b). To elucidate the mechanisms underlying these anomalies, daily hypolimnetic temperatures simulated by W2 were adopted as targets to develop specific XGBoost models for early (May–June), mid (July–August), and late (September–October) stratified periods. SHAP analysis was then applied to quantify the dominant predictors in each interval.

The period-specific XGBoost models satisfactorily reproduced CE-QUAL-W2 hypolimnetic temperatures with RMSE of 0.08, 0.09 and 0.13 °C for early, mid and late stratification, respectively ($R^2 = 0.96–0.98$). The results further demonstrate pronounced stage-dependent shifts in the controls on hypolimnetic temperature (Fig. 9). Specifically, during the early-stratified period (May–June) the 30-day antecedent mean air temperature, outflow discharge and wind direction emerge as the three leading drivers. By mid-stratification (July–August) the principal controls change over to the 30-day mean short-wave irradiance followed by outflow discharge, whereas in the late-stratified phase (September–October) the positive influence of outflow discharge becomes overwhelmingly dominant (Fig. 9): its SHAP contribution attains 0.513—over four times greater than that of air temperature (0.131, ranked second) and shortwave radiation (0.115, ranked third). To corroborate this finding, we examined years in which late-season hypolimnetic temperatures were anomalously elevated.

https://doi.org/10.5194/egusphere-2025-6442
Preprint. Discussion started: 20 February 2026

In 1981, 2001, 2002, and 2007, the median discharge during late stratification was 5.24 $m^3 s^{-1}$, approximately 125% higher than the 40-year median (2.32 $m^3 s^{-1}$) for this interval, a difference that was statistically significant (Dunn's test, $p < 0.05$, see Fig.8a). Furthermore, during this period, the SHAP contribution of outflow discharge was also markedly greater than those of the other predictors (Fig. 9d). Collectively, the hydrological signature provides independent evidence that enhanced release discharge is the key driver of late-stratification hypolimnetic warming.

4. Discussion

4.1. Reconstruction of thermal structure from multi-decadal full-profile observations

In this study we assembled a uniquely long and vertically resolved data set comprising almost four decades (1981–2019) of temperature profiles (0–70 m) and concomitant meteorological forcing for Rappbode Reservoir, the largest drinking water reservoir in Germany. On this basis, we established an analytical framework, combinng process-based (CE-QUAL-W2) and data-driven (XGBoost) models, to systematically assess their capabilities in reproducing the reservoir's thermal structure. Whereas most publicly available lake- and reservoir-temperature records span ≤ 10 years and rarely include deep-water observations for long-term periods (Ladwig et al. 2021; Woolway et al. 2020), the present data set bridges an inter-decadal gap and thus provides an exceptional resource for full-profile hydrodynamic modelling.

Here, the 39-year observations and simulations consistently indicate a pronounced epilimnetic warming of the reservoir, with observed and simulated warming rates of 0.06 and 0.05 °C a^{-1}, respectively, which closely matches-and even marginally exceeds-the concurrent

https://doi.org/10.5194/egusphere-2025-6442
Preprint. Discussion started: 20 February 2026

increase in regional air temperature (0.04 °C yr^{-1}; Mann–Kendall test, $p = 0.001$) and the pan-European synthesis of temperate lakes (O'Reilly et al. 2015; Shatwell et al. 2019). In contrast, deep-water temperatures at 30m and 50m depth exhibited no significant trends, thereby reflecting a characteristic pattern of intensified surface warming concurrent with relatively stable deep-water temperatures. This vertical asymmetry in warming preserves the cold-water refuge but implies a strengthening of thermal stratification. Numerous studies have shown that such shifts in lake and reservoir thermodynamics would exacerbate hypolimnetic anoxia and enhances internal nitrogen and phosphorus loading (Sun et al. 2022; Weinke and Biddanda 2019), subsequently impairing source-water quality and downstream aquatic ecosystems (Jane et al. 2023). Accordingly, coupling the validated thermal models with biogeochemical modules to quantify present-day and future trajectories of dissolved oxygen, and to develop targeted water-quality management strategies, constitutes a logical and necessary extension of the current work.

4.2. Atmospheric and hydraulic drivers governing thermal dynamics in stratified reservoirs

The SHAP values indicated that the antecedent 30-day mean air temperature is the most influential predictor of epilimnetic temperature, as well as of Schmidt stability and the bottom-to-surface temperature difference, followed by dew-point temperature and shortwave radiation. This hierarchy corroborates earlier findings derived from short-term datasets for dimictic lakes by Livingstone and Lotter (1998) and Darko et al. (2019), and is now quantitatively confirmed by our 39-year observational record. All such results highlight the lagged response of the three surface-heat-forced stratification metrics to cumulative antecedent heat fluxes (i.e., the thermal

https://doi.org/10.5194/egusphere-2025-6442
Preprint. Discussion started: 20 February 2026

inertia effect). Here, the epilimnetic thermal inertia τ is defined as (Imberger and Patterson 1989):

$$\tau = \frac{\rho\, c_p\, h}{H_{net}} \qquad (3)$$

where ρ is water density, c_p the specific heat capacity (4.18×10^3 J kg^{-1} K^{-1}), h the mixed-layer depth and H_{net} the daily-mean net heat flux. For Rappbode Reservoir, according to the thermal conditions during the stratified period (Mi et al. 2019), ρ is defined as 998 kg m^{-3}, h is from 9 m to 11 m, and H_{net} is from 18 W m^{-2} to 24 W m^{-2} which yields τ ranging from 25d to 29d, in close agreement with the 30-day averaging window that dominates the SHAP ranking. Because this response time exceeds the characteristic 1-day scale of surface heat-flux variability by an order of magnitude, daily atmospheric perturbations are strongly filtered by thermal inertia and thus contribute little to the statistical ranking.

By comparison, in the hypolimnion (30–50 m), short-wave radiation exceeds air temperature as the dominant predictor, and the SHAP importance of outflow discharge concurrently increases, because sustained deep withdrawals remove the coldest layers, erode thermocline stability and induce compensation flows that advect warmer water downward (Olsson 2021; Weber et al. 2017), thereby regulating hypolimnetic temperature. Our analysis further reveals that, for mixed-layer depth, outflow discharge emerges as the second-most influential predictor. As shown above, this can be attributed to sustained hypolimnetic withdrawals, which induce downward flows and consequently deepen the mixed layer (Deng et al. 2011; Mi et al. 2023a). Additionally, the role of cloud cover should not be overlooked (ranking fourth in SHAP values), since cloudiness can effectively modulate incoming shortwave and longwave radiation, thus altering surface buoyancy fluxes (Boehrer and

https://doi.org/10.5194/egusphere-2025-6442
Preprint. Discussion started: 20 February 2026

Schultze 2008).

4.3. Late-season hypolimnetic warming— mechanistic insights from period-specific SHAP analysis

During late stratification, increased deep-layer withdrawals are more effective at warming the hypolimnion for two complementary reasons. First, over this period, nocturnal cooling and declining net radiation substantially reduce Schmidt stability to $< 1 \times 10^3$ J m^{-2} (Fig. 5), compared with $> 2 \times 10^3$ J m^{-2} in midsummer (July–August), weakening the density interface so that mixing event can more easily penetrate the metalimnion and transport heat downward. Second, the mixed layer deepens from about 6 m in early summer to 18 m by September-October (Fig. S4), thereby reducing the vertical distance between the mixed-layer base and the water-withdrawal intake (at the depths of 60–70 m) by ≈20%. The compensatory inflow therefore traverses a shorter pathway with lower viscous and buoyancy dissipation, allowing a larger fraction of warm water to reach hypolimnion (Feldbauer et al. 2020). The concurrence of a weakened density interface and a contracted transport pathway explains why high-discharge deep withdrawals can rapidly elevate bottom temperatures during late stratification.

Despite pronounced hypolimnetic warming induced by deep-water withdrawals in the late stratification periods of 1981, 2001, 2002, and 2007, the surface-to-bottom temperature difference remained above 1 °C for most of October (Fig. S5), indicating persistent and stable stratification conditions (Fang and Stefan 2009). Hypolimnetic warming under such weakened stratification poses a severe ecological threat since oxygen demand in the hypolimnion increases sharply with temperature while atmospheric re-oxygenation remains inhibited. For

https://doi.org/10.5194/egusphere-2025-6442
Preprint. Discussion started: 20 February 2026

Rappbode Reservoir, our previous work suggested that raising bottom-water temperature from a typical 6 °C to 10 °C (October 2001) augments the sediment oxygen demand (SOD) from 0.46 to 1.04 g O_2 m^{-2} d^{-1} (Mi et al. 2020). Under a persistent density barrier, this additional demand cannot be offset by oxygen replenishment from surface waters, greatly amplifying the risk of hypolimnetic anoxia. Such adverse effects associated with a "warm yet stratified" state have also been systemically documented at the CW Bill Young Regional Reservoir (Bryant et al. 2024), and Cedar Lake (James et al. 2015), USA. Taken together, these observations underscore the management relevance of hypolimnetic warming during late-season stratification decay; accordingly, future work should quantify threshold conditions that link this warming to hypolimnetic oxygen debt—e.g., stability and withdrawal-rate percentiles—and test operational adaptation strategies that minimize exposure to this state.

4.4. An integrated analytical framework for long-term thermal reconstruction and driver attribution

Our study not only clarifies the thermal dynamics of reservoirs and their external drivers, but also introduces a new methodology that is of broader interest. By assimilating routine observations into a site-calibrated CE-QUAL-W2 model, we reconstruct a four-decade, depth-resolved (0–70 m) temperature archive with high vertical and temporal resolution, transforming sparse monitoring into continuous vertical profiles for subsequent analyses. Second, an interpretable machine-learning workflow (XGBoost with rolling-origin cross-validation and early stopping) provides fast, accurate prediction across depths, which is directly relevant for forecasting use-cases increasingly requested by reservoir managers (Carey et al. 2022). Third, the SHAP analysis provides additive, model-consistent attributions that decompose any

https://doi.org/10.5194/egusphere-2025-6442
Preprint. Discussion started: 20 February 2026

thermal anomaly into depth- and sample-specific contributions of individual drivers. In practice, this yields a quantitative explanation of reservoir thermal anomalies without running time-consuming large scenario ensembles with the process model.

Collectively, these advantages constitute an integrated mechanistic–statistical framework that is readily transferable to other stratified lakes and reservoirs for long-term thermal reconstruction, driver attribution and operational evaluation.

5. Conclusion

- We developed an integrated CE-QUAL-W2 and machine-learning framework that reliably reconstructs, over nearly four decades, the full-depth thermal structure of Rappbode Reservoir, capturing the spatiotemporal variability of layer-specific temperatures and stratification-strength metrics.
- SHAP attribution based on the integrated framework revealed strong vertical heterogeneity in the controls on reservoir thermodynamics: surface temperature was governed primarily by the antecedent 30-day means of air temperature, dew-point temperature, and incident shortwave radiation, whereas the influence of shortwave radiation and outflow discharge increased progressively with depth and the relative effect of air temperature strongly declined.
- The dominant controls on bottom-water temperature shifted systematically across stratification phases: during early stratification (May–June), the leading drivers were the antecedent 30-day mean air temperature, outflow discharge, and wind direction; during mid stratification (July–August), shortwave radiation and outflow discharge jointly dominated; during late stratification (September–October), outflow discharge became the

https://doi.org/10.5194/egusphere-2025-6442
Preprint. Discussion started: 20 February 2026

overwhelming control, with a SHAP contribution more than four times that of air temperature and shortwave radiation.

- Observations and simulations consistently showed that bottom-water temperature rose anomalously to ~10 °C during late stratification in 1981, 2001, 2002, and 2007, whereas it typically remained at 4–6 °C in other years. Further analyses indicated that these events were primarily triggered by intensified deep withdrawals in late stratification, with outflow discharge ~2.25 times higher than in typical years. The enhanced discharge weakened the density gradient and strengthened downward compensatory transport, driving the bottom-water thermal anomaly.

Code and data availability

The source code of the model CE-QUAL-W2 can be freely downloaded at http://cee.pdx.edu/w2/. All the datasets that support the findings of this study are available from the corresponding author upon reasonable request.

Authors' contributions

CM conducted the W2 modeling approach, with the help from BG. CM, XK and YJ analyzed data and wrote the manuscript. CNC and KR reviewed, edited and proofread the manuscript. All authors read and approved the final manuscript.

Competing interests

https://doi.org/10.5194/egusphere-2025-6442
Preprint. Discussion started: 20 February 2026

The authors declare that they have no conflict of interest.

Acknowledgements

This work was supported by National Natural Science Foundation of China (42577078, 42177062), National Key Research and Development Program of China (2023YFF0807203), Science and Technology Projects of Xizang Autonomous Region, China (XZ202501ZY0091) and International Partnership Program of Chinese Academy of Sciences (IPP)(045GJHZ2023055FN). XK was also supported by the "Hundred People Program" of the Chinese Academy of Sciences.

https://doi.org/10.5194/egusphere-2025-6442
Preprint. Discussion started: 20 February 2026

Reference

Akbari, E., S. K. Alavipanah, M. Jeihouni, M. Hajeb, D. Haase & S. Alavipanah, 2017. A review of ocean/sea subsurface water temperature studies from remote sensing and non-remote sensing methods. Water 9(12):936.

Anderson, E., C. Stow, A. Gronewold, L. Mason, M. McCormick, S. Qian, S. Ruberg, K. Beadle, S. Constant & N. Hawley, 2021. Seasonal overturn and stratification changes drive deep-water warming in one of Earth's largest lakes. Nature Communications 12 doi:10.1038/s41467-021-21971-1.

Bertone, E., R. A. Stewart, H. Zhang, M. Bartkow & C. Hacker, 2015. An autonomous decision support system for manganese forecasting in subtropical water reservoirs. Environmental Modelling & Software 73:133-147.

Boehrer, B. & M. Schultze, 2008. Stratification of lakes. Rev Geophy 46:RG 2005 doi:10.1029/2006RG000210.

Boehrer, B. & M. Schultze, 2009. Density Stratification and Stability.

Bouffard, D., J. D. Ackerman & L. Boegman, 2013. Factors affecting the development and dynamics of hypoxia in a large shallow stratified lake: Hourly to seasonal patterns. Water Resources Research 49(5):2380-2394.

Bryant, L. D., N. Brockbank & D. Austin, 2024. To mix or not to mix? A holistic approach to stratification-preserving and destratification aeration of drinking-water supply reservoirs. Water Research 261:121974.

Carey, C. C., W. M. Woelmer, M. E. Lofton, R. J. Figueiredo, B. J. Bookout, R. S. Corrigan, V. Daneshmand, A. G. Hounshell, D. W. Howard & A. S. Lewis, 2022. Advancing lake and reservoir water quality management with near-term, iterative ecological forecasting. Inland Waters 12(1):107-120.

Carr, M. K., A. Sadeghian, K.-E. Lindenschmidt, K. Rinke & L. Morales-Marin, 2019. Impacts of Varying Dam Outflow Elevations on Water Temperature, Dissolved Oxygen, and Nutrient Distributions in a Large Prairie Reservoir. Environ Eng Sci.

Cole, T. M. & S. A. Wells, 2006. CE-QUAL-W2: A two-dimensional, laterally averaged, hydrodynamic and water quality model, version 3.5.

Darko, D., D. Trolle, R. Asmah, K. Bolding, K. A. Adjei & S. N. Odai, 2019. Modeling the impacts of climate change on the thermal and oxygen dynamics of Lake Volta. Journal of Great Lakes Research 45(1):73-86.

Deka, P. P. & J. Weiner, 2024. XGBoost for Regression Predictive Modeling and Time Series Analysis: Learn how to build, evaluate, and deploy predictive models with expert guidance. Packt Publishing Ltd.

Deng, Y., Y. Tuo, J. Li, K. Li & R. Li, 2011. Spatial-temporal effects of temperature control device of stoplog intake for Jinping I hydropower station. Science China Technological Sciences 54(1):83-88.

Dong, F., C. Mi, M. Hupfer, K. E. Lindenschmidt, W. Peng, X. Liu & K. Rinke, 2019. Assessing vertical diffusion in a stratified lake using a 3D hydrodynamic model. Hydrological Processes.

Fang, X. & H. G. Stefan, 2009. Simulations of climate effects on water temperature, dissolved oxygen, and ice and snow covers in lakes of the contiguous United States under past and future climate scenarios. Limnology and Oceanography 54:2359-2370.

Feldbauer, J., D. Kneis, T. Hegewald, T. U. Berendonk & T. Petzoldt, 2020. Managing climate change in drinking water reservoirs: potentials and limitations of dynamic withdrawal strategies. Environmental Sciences Europe 32(1):48 doi:10.1186/s12302-020-00324-7.

Imberger, J. & J. C. Patterson, 1989. Physical limnology. Adv Appl Mech 27:303-475.

James, W. F., P. W. Sorge & P. J. Garrison, 2015. Managing internal phosphorus loading and vertical entrainment

https://doi.org/10.5194/egusphere-2025-6442
Preprint. Discussion started: 20 February 2026

in a weakly stratified eutrophic lake. Lake Reserv Manage 31(4):292-305.

Jane, S. F., J. L. Mincer, M. P. Lau, A. S. Lewis, J. T. Stetler & K. C. Rose, 2023. Longer duration of seasonal stratification contributes to widespread increases in lake hypoxia and anoxia. Global Change Biology 29(4):1009-1023.

Kirillin, G. & T. Shatwell, 2016. Generalized scaling of seasonal thermal stratification in lakes. Earth-sci Rev 161:179-190.

Kobler, U. G., A. Wüest & M. Schmid, 2018. Combined effects of pumped-storage operation and climate change on thermal structure and water quality. Climatic Change doi:10.1007/s10584-018-2340-x.

Kreakie, B., S. Shivers, J. Hollister & W. Milstead, 2021. Predictive model of lake photic zone temperature across the conterminous United States. Frontiers in environmental science 9:707874.

LaBrie, R., M. Hupfer & M. P. Lau, 2023. Anaerobic duration predicts biogeochemical consequences of oxygen depletion in lakes. Limnology and Oceanography Letters 8(4):666-674.

Ladwig, R., P. C. Hanson, H. A. Dugan, C. C. Carey, Y. Zhang, L. Shu, C. J. Duffy & K. M. Cobourn, 2021. Lake thermal structure drives interannual variability in summer anoxia dynamics in a eutrophic lake over 37 years. Hydrology and Earth System Sciences 25(2):1009-1032.

Lewis Jr, W. M., J. H. McCutchan Jr & J. Roberson, 2019. Effects of climatic change on temperature and thermal structure of a mountain reservoir. Water Resources Research 55(3):1988-1999.

Li, Z., Z. Zhang, S. Xiong, W. Zhang & R. Li, 2024. Lake Surface Temperature Predictions under Different Climate Scenarios with Machine Learning Methods: A Case Study of Qinghai Lake and Hulun Lake, China. Remote Sensing 16(17):3220.

Livingstone, D. M. & A. F. Lotter, 1998. The relationship between air and water temperatures in lakes of the Swiss Plateau: a case study with pal\sgmaelig; olimnological implications. J Paleolimnol 19:181-198.

Lundberg, S. M., G. Erion, H. Chen, A. DeGrave, J. M. Prutkin, B. Nair, R. Katz, J. Himmelfarb, N. Bansal & S.-I. Lee, 2020. From local explanations to global understanding with explainable AI for trees. Nature machine intelligence 2(1):56-67.

Lyu, H., N. Sha, S. Qin, M. Yan, Y. Xie & R. Wang, 2019. Advances in neural information processing systems. Adv Neural Inf Process Syst 32.

Meinson, P., A. Idrizaj, P. Nõges, T. Nõges & A. Laas, 2016. Continuous and high-frequency measurements in limnology: history, applications, and future challenges. Environ Rev 24(1):52-62.

Mi, C., M. A. Frassl, B. Boehrer & K. Rinke, 2018. Episodic wind events induce persistent shifts in the thermal stratification of a reservoir (Rappbode Reservoir, Germany). International Review of Hydrobiology 103:71-82.

Mi, C., D. P. Hamilton, M. A. Frassl, T. Shatwell, X. Kong, B. Boehrer, Y. Li, J. Donner & K. Rinke, 2022. Controlling blooms of Planktothrix rubescens by optimized metalimnetic water withdrawal: a modelling study on adaptive reservoir operation. Environmental Sciences Europe 34(1):1-16.

Mi, C., K. Rinke & T. Shatwell, 2023a. Optimizing selective withdrawal strategies to mitigate hypoxia under water-level reduction in Germany's largest drinking water reservoir. JEnvS.

Mi, C., A. Sadeghian, K.-E. Lindenschmidt & K. Rinke, 2019. Variable withdrawal elevations as a management tool to counter the effects of climate warming in Germany's largest drinking water reservoir. Environmental Sciences Europe 31(1):19.

Mi, C., T. Shatwell, X. Kong & K. Rinke, 2023b. Cascading climate effects in deep reservoirs: Full assessment of physical and biogeochemical dynamics under ensemble climate projections and ways towards adaptation. Ambio doi:10.1007/s13280-023-01950-0.

Mi, C., T. Shatwell, J. Ma, V. C. Wentzky, B. Boehrer, Y. Xu & K. Rinke, 2020. The formation of a metalimnetic

https://doi.org/10.5194/egusphere-2025-6442
Preprint. Discussion started: 20 February 2026

oxygen minimum exemplifies how ecosystem dynamics shape biogeochemical processes: A modelling study. Water Research.

Nkwalale, L., R. Schwefel, M. Yaghouti & K. Rinke, 2023. A simple model for predicting oxygen depletion in lakes under climate change. Inland Waters 13(4):576-595.

Noori, R., R. I. Woolway, C. Jun, S. M. Bateni, D. Naderian, S. Partani, M. Maghrebi & M. Pulkkanen, 2023. Multi-decadal change in summer mean water temperature in Lake Konnevesi, Finland (1984–2021). Ecol Inform 78:102331 doi:https://doi.org/10.1016/j.ecoinf.2023.102331.

O'Reilly, C. M., S. Sharma, D. K. Gray, S. E. Hampton, J. S. Read, R. J. Rowley, P. Schneider, J. D. Lenters, P. B. McIntyre & B. M. Kraemer, 2015. Rapid and highly variable warming of lake surface waters around the globe. Geophysical Research Letters 42(24):10,773-10,781 doi:http://dx.doi.org/10.1002/2015GL066235.

Oleksy, I. A. & D. C. Richardson, 2021. Climate change and teleconnections amplify lake stratification with differential local controls of surface water warming and deep water cooling. Geophysical Research Letters 48(5):e2020GL090959.

Olsson, F., 2021. Impacts of water residence time on lake thermal structure: Implications for management and climate change. Lancaster University (United Kingdom).

Pilla, R. M., E. M. Mette, C. E. Williamson, B. V. Adamovich, R. Adrian, O. Anneville, E. Balseiro, S. Ban, S. Chandra & W. Colom-Montero, 2021. Global data set of long-term summertime vertical temperature profiles in 153 lakes. scientific data 8(1):200.

Rinke, K., B. Kuehn, S. Bocaniov, K. Wendt-Potthoff, O. Buttner, J. Tittel, M. Schultze, P. Herzsprung, H. Ronicke, K. Rink, K. Rinke, M. Dietze, M. Matthes, L. Paul & K. Friese, 2013. Reservoirs as sentinels of catchments: the Rappbode Reservoir Observatory (Harz Mountains, Germany). Environmental Earth Sciences 69(2):523-536 doi:http://dx.doi.org/10.1007/s12665-013-2464-2.

Schwefel, R., L. G. Nkwalale, S. Jordan, K. Rinke & M. Hupfer, 2025. Temperatures and hypolimnetic oxygen in German lakes: Observations, future trends and adaptation potential. Ambio 54(3):428-447.

Sharma, S., D. K. Gray, J. S. Read, C. M. O'reilly, P. Schneider, A. Qudrat, C. Gries, S. Stefanoff, S. E. Hampton & S. Hook, 2015. A global database of lake surface temperatures collected by in situ and satellite methods from 1985–2009. Scientific data 2(1):1-19.

Shatwell, T., W. Thiery & G. Kirillin, 2019. Future projections of temperature and mixing regime of European temperate lakes. Hydrology and Earth System Sciences 23(3):1533-1551.

Sun, C., S. Wang, H. Wang, X. Hu, F. Yang, M. Tang, M. Zhang & J. Zhong, 2022. Internal nitrogen and phosphorus loading in a seasonally stratified reservoir: Implications for eutrophication management of deep-water ecosystems. Journal of Environmental Management 319:115681.

Weber, M., K. Rinke, M. Hipsey & B. Boehrer, 2017. Optimizing withdrawal from drinking water reservoirs to reduce downstream temperature pollution and reservoir hypoxia. Journal of Environmental Management 197:96-105.

Weinke, A. D. & B. A. Biddanda, 2019. Influence of episodic wind events on thermal stratification and bottom water hypoxia in a Great Lakes estuary. Journal of Great Lakes Research 45(6):1103-1112.

Wentzky, V. C., J. Tittel, C. G. Jäger & K. Rinke, 2018. Mechanisms preventing a decrease in phytoplankton biomass after phosphorus reductions in a German drinking water reservoir—results from more than 50 years of observation. Freshwater biology 63(9):1063-1076 doi:http://dx.doi.org/10.1111/fwb.13116.

Woolway, R. I., M. B. Kayastha, Y. Tong, L. Feng, H. Shi & P. Xue, 2025. Subsurface heatwaves in lakes. Nature Climate Change 15(5):554-559 doi:10.1038/s41558-025-02314-0.

Woolway, R. I., B. M. Kraemer, J. D. Lenters, C. J. Merchant, C. M. O'Reilly & S. Sharma, 2020. Global lake

https://doi.org/10.5194/egusphere-2025-6442
Preprint. Discussion started: 20 February 2026

responses to climate change. Nature Reviews Earth & Environment 1(8):388-403.

https://doi.org/10.5194/egusphere-2025-6442
Preprint. Discussion started: 20 February 2026

Figures

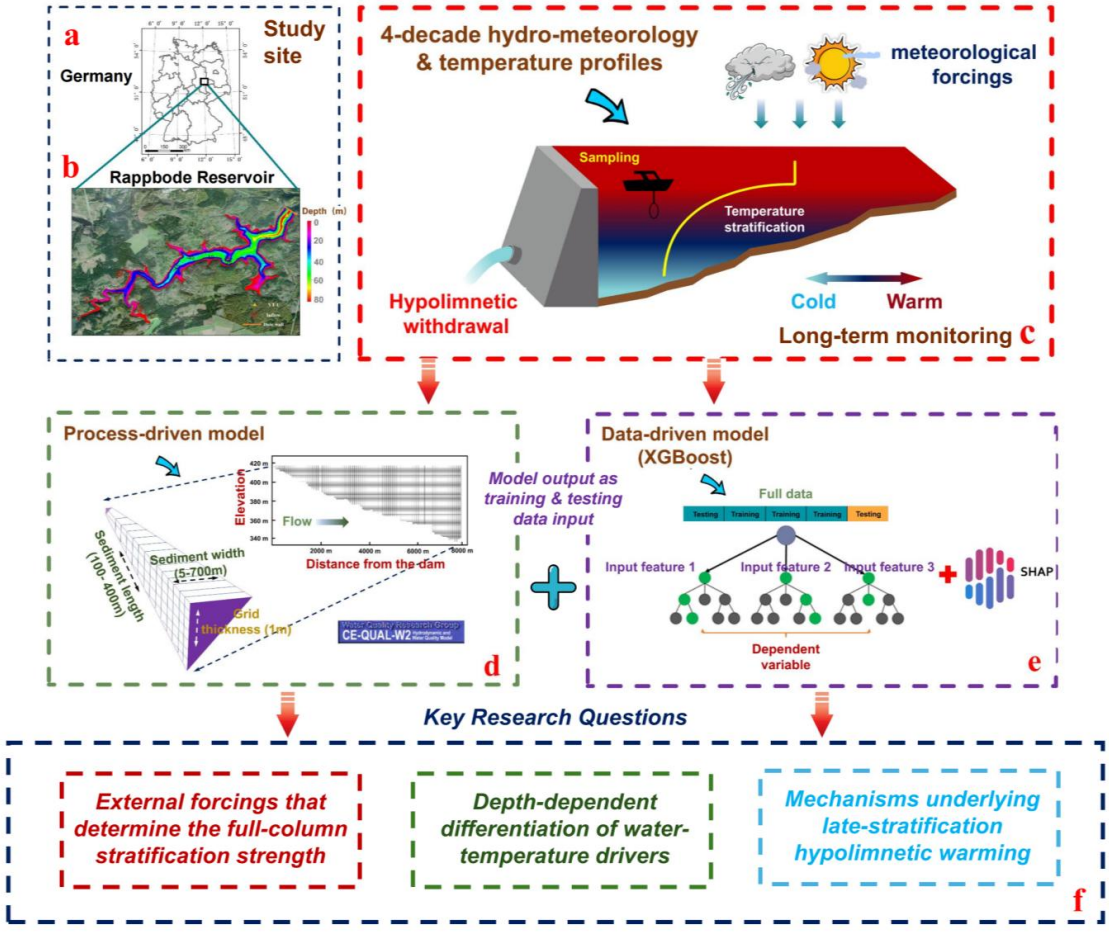

Fig. 1. (a) Location of the Rappbode Reservoir in Germany. (b) Reservoir bathymetry and the long-term water-temperature monitoring site (YT1). (c–e) Data flow and model coupling within the integrated analytical framework: (c) four decades of hydrometeorological forcings and in-lake temperature profiles; (d) process-based modeling with CE-QUAL-W2; (e) interpretable machine learning with XGBoost/SHAP; and (f) key question addressed in this study.

https://doi.org/10.5194/egusphere-2025-6442
Preprint. Discussion started: 20 February 2026

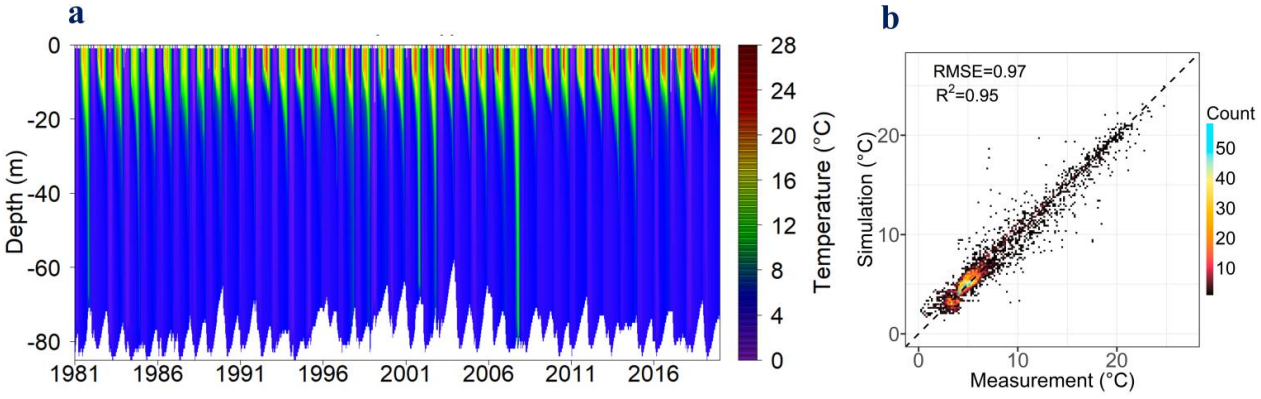

Fig. 2. (a) Thermal dynamics of Rappbode Reservoir, from W2 simulation results, during the study period; (b) Comparison between simulated and observed water temperature with the colour scale denoting the number of samples per hexagon. The dashed line represents the 1:1 line.

https://doi.org/10.5194/egusphere-2025-6442
Preprint. Discussion started: 20 February 2026

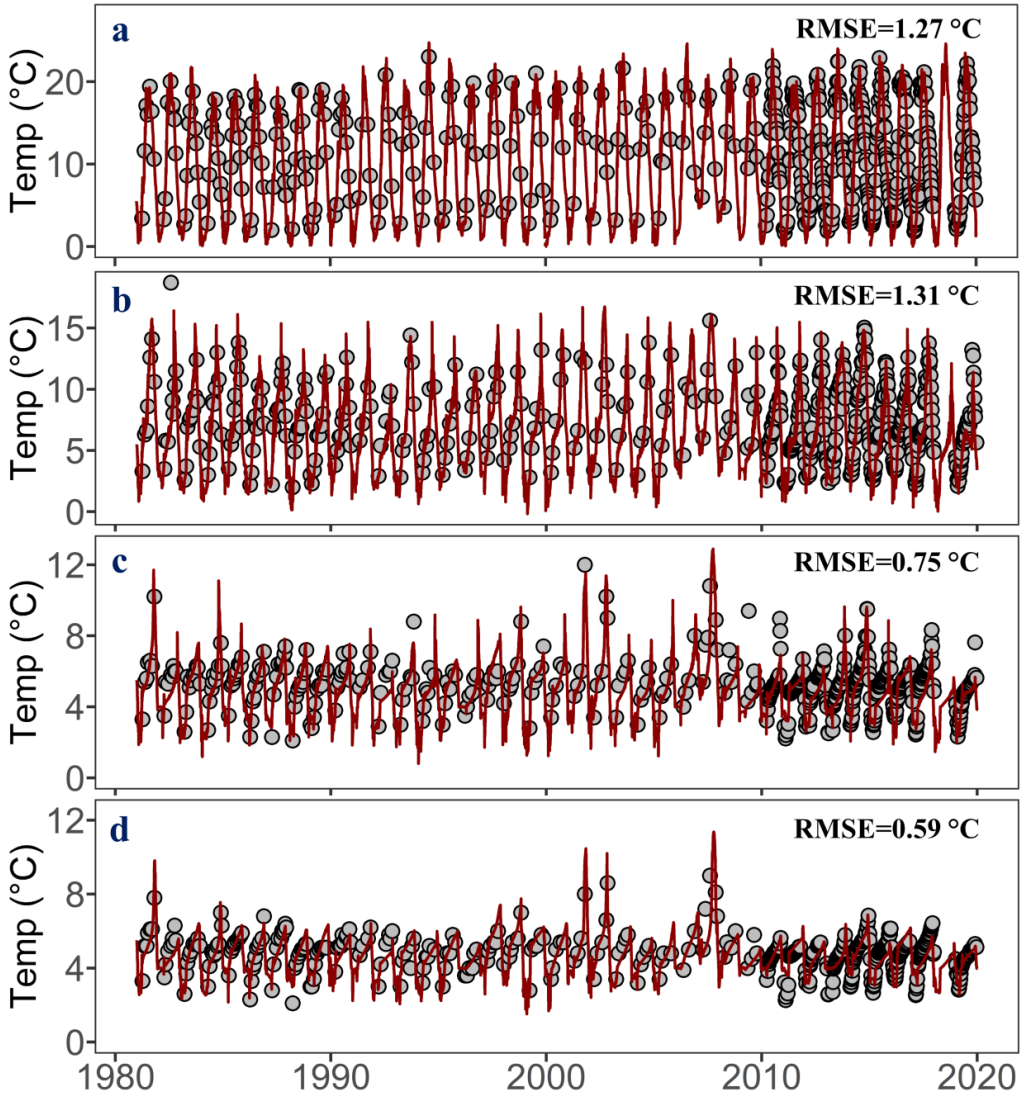

Fig. 3. Observed (grey circles) versus simulated (black line) water temperatures in the Rappbode Reservoir at 5 m (a), 15 m (b), 30 m (c), and 50 m (d). The RMSE for each panel is shown in the upper-right corner.

https://doi.org/10.5194/egusphere-2025-6442
Preprint. Discussion started: 20 February 2026

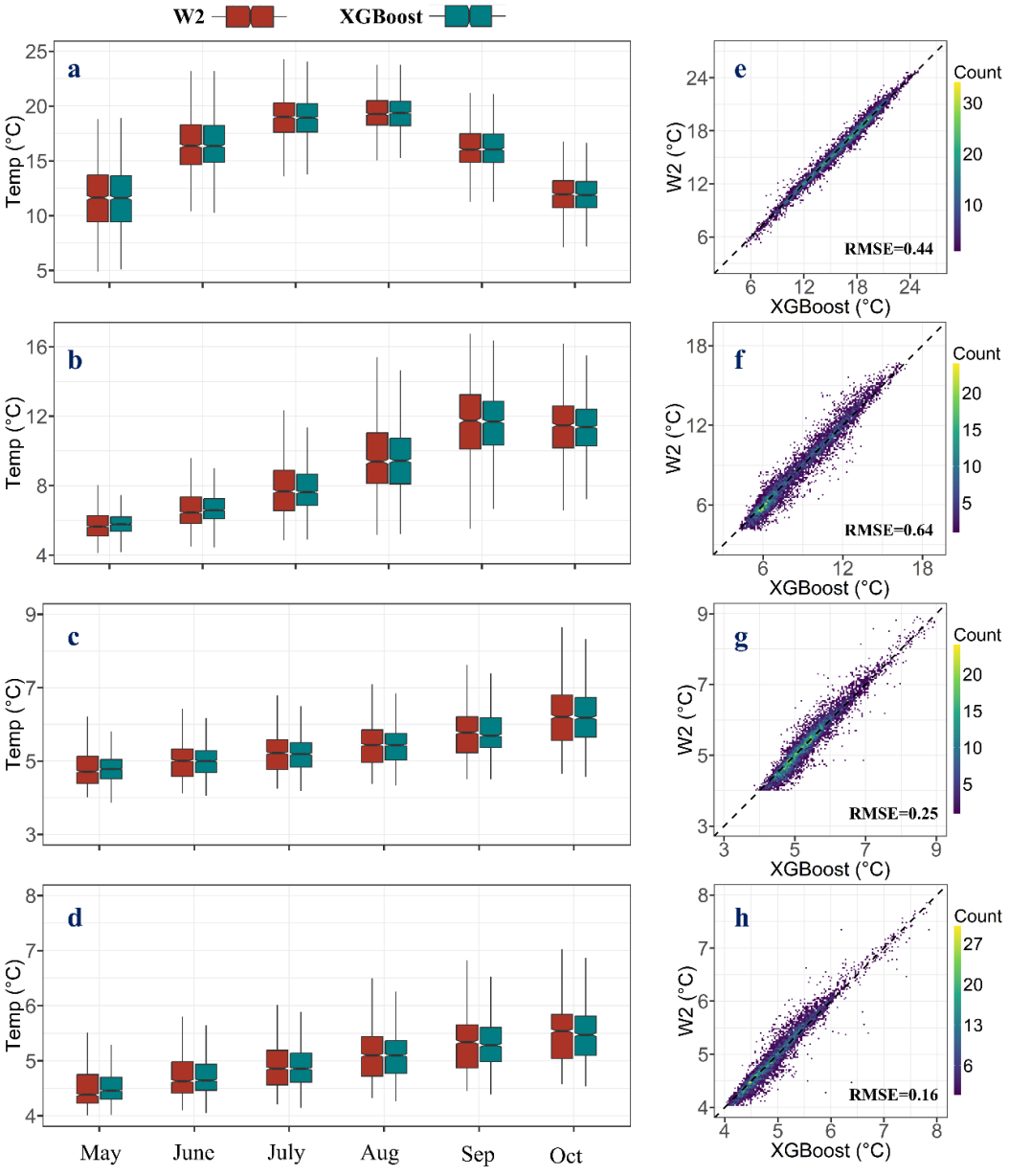

Fig. 4. Water temperature simulated by W2 and XGBoost in Rappbode Reservoir at the depth of 5m (a), 15m (b), 30m (c) and 50m (d), with the right column indicating the comparison for all specific depths.

https://doi.org/10.5194/egusphere-2025-6442
Preprint. Discussion started: 20 February 2026

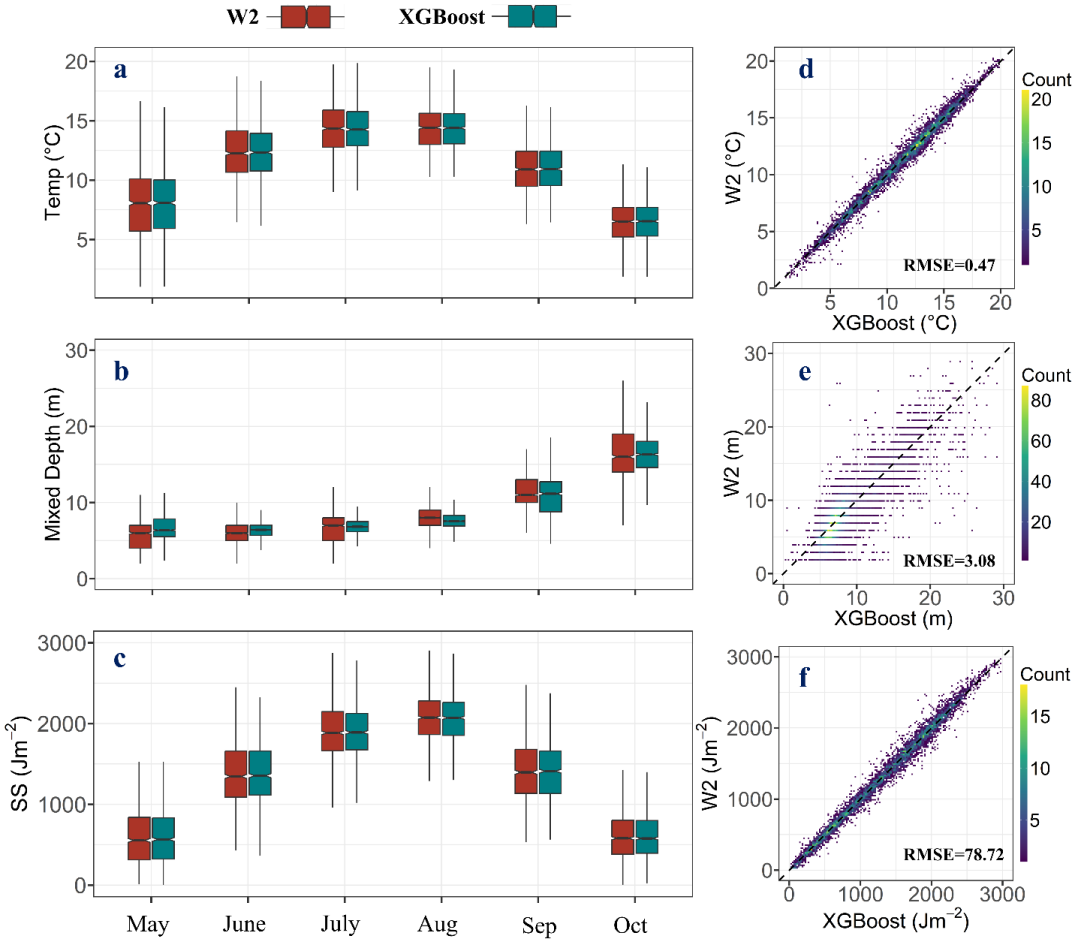

Fig. 5. Stratification dynamics simulated by W2 and XGBoost in Rappbode Reservoir for bottom-to-surface temperature difference (a), mixed-layer depth (b) and Schmidt Stability (c), with the right column indicating the comparison for the three indexes.

https://doi.org/10.5194/egusphere-2025-6442
Preprint. Discussion started: 20 February 2026

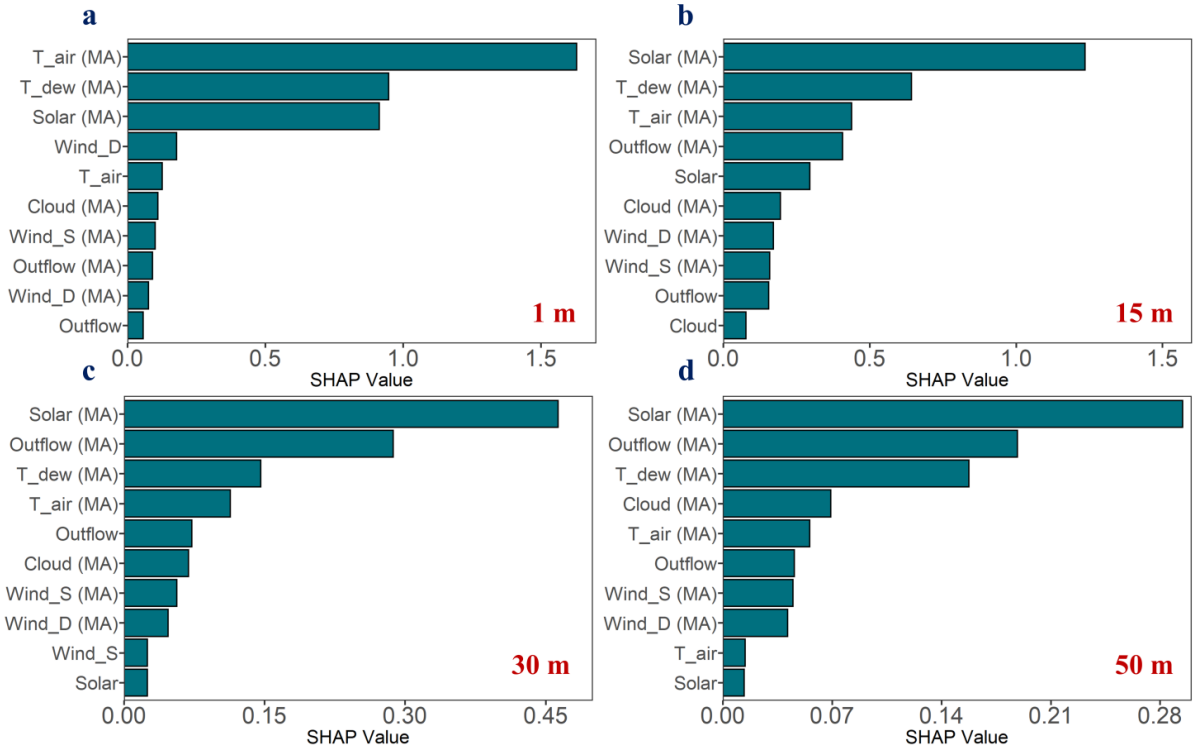

Fig. 6. Driving factors analysis for water temperature at the depth of 5m (a), 15m (b), 30m (c) and 50m (d) based on the SHAP values. MA indicates moving-average features.

https://doi.org/10.5194/egusphere-2025-6442
Preprint. Discussion started: 20 February 2026

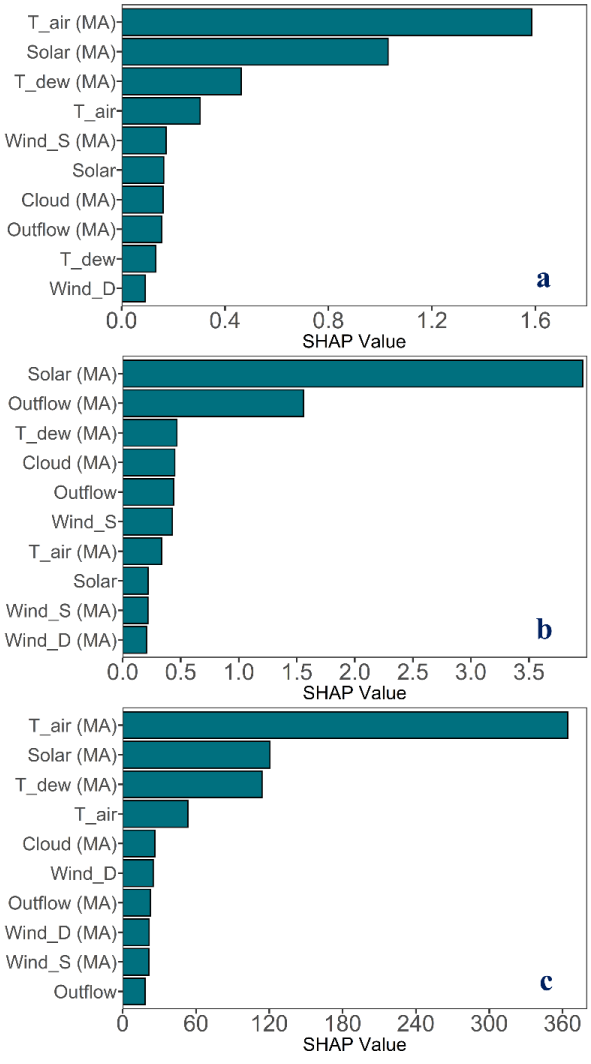

Fig. 7. Driving factors analysis for bottom-to-surface temperature difference (a), mixed-layer depth (b) and Schmidt Stability (c), based on the SHAP values. MA indicates moving-average features.

https://doi.org/10.5194/egusphere-2025-6442
Preprint. Discussion started: 20 February 2026

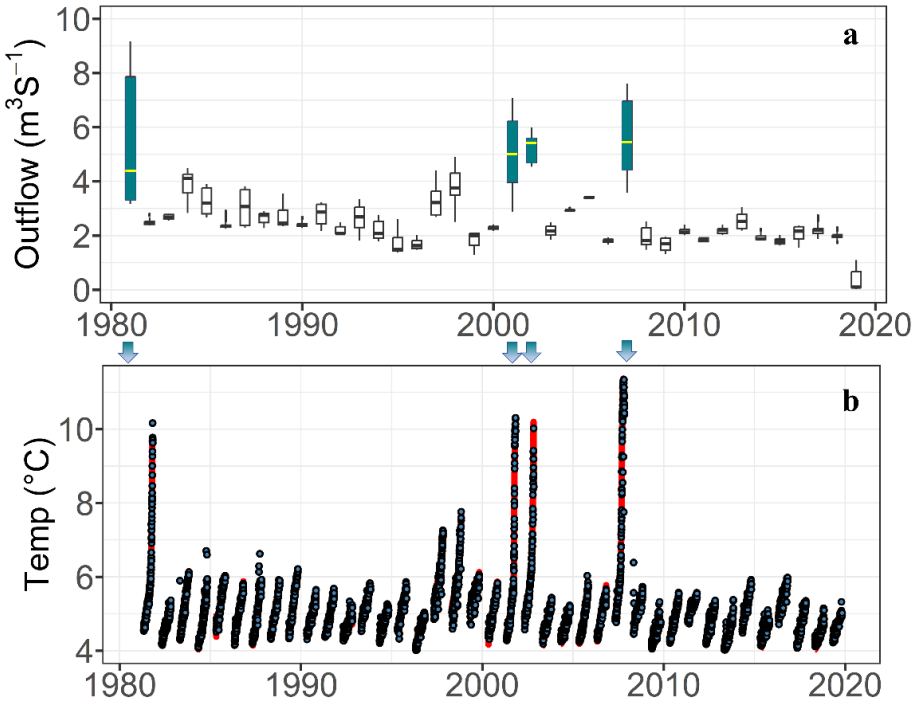

Fig. 8. (a) Moving-average of discharge during September–October for each year (with 1981, 2001, 2002, and 2007 highlighted in green); (b) water temperature, at the depth of 50m, from W2 (red lines) and XGBoost (black point) for each year.

https://doi.org/10.5194/egusphere-2025-6442
Preprint. Discussion started: 20 February 2026

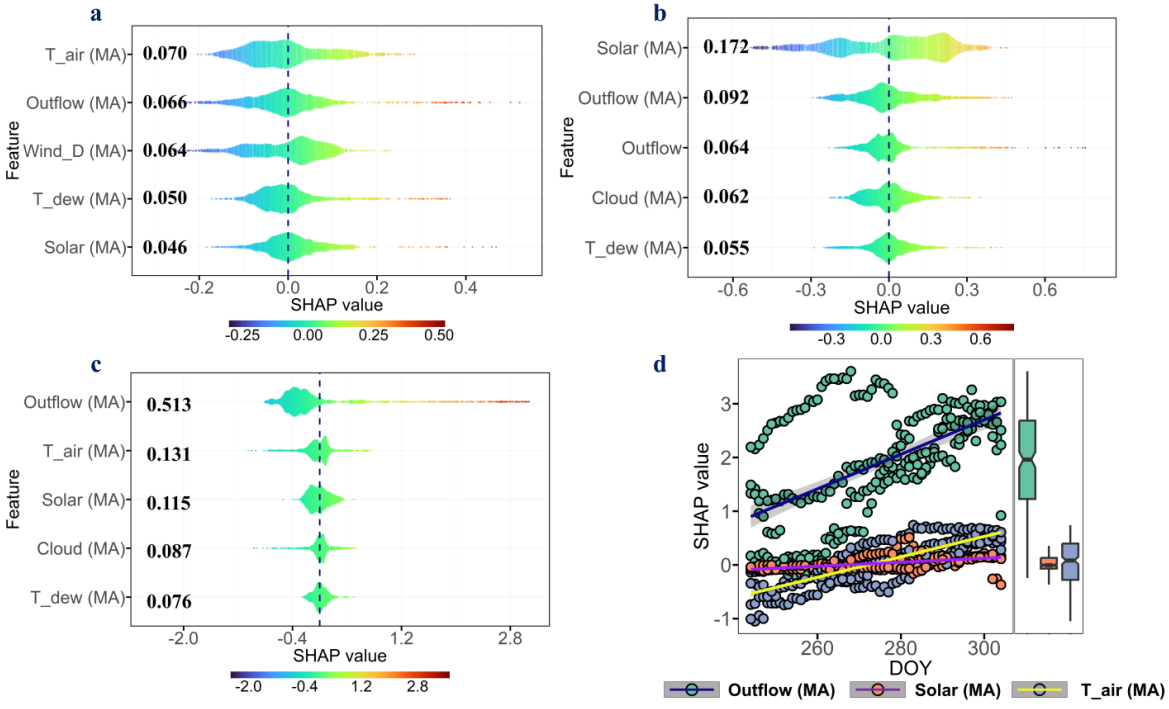

Fig. 9. Comparison of SHAP-derived driver importance for bottom-layer water temperature at 50 m depth. (a–c) SHAP value rankings showing how dominant drivers vary across the initial (May–June), middle (July–August), and final (September–October) stages of stratification. (d) Comparison of SHAP values during September–October for outflow (green), solar radiation (red), and air temperature (blue) in 1981, 2001, 2002, and 2007; points denote daily values plotted against day of year (DOY), with colored lines indicating linear regression fits, and adjacent boxplots summarizing the corresponding distributions. MA indicates moving-average features.